Electronic Supplementary Information for

Nanoreactors stable up to 200°C: A class of high temperature microemulsions composed solely of ionic liquids

Yuanchao Pei*[a], Jie Ru[a], Kaisheng Yao[b], Lihui Hao[a], Zhiyong Li[a], Huiyong Wang[a], Xingqi Zhu[c] and Jianji Wang*[a]

[a]*Henan Key Laboratory of Green Chemistry, Collaborative Innovation Center of Henan Province for Green Manufacturing of Fine Chemicals, Key Laboratory of Green Chemical Media and Reactions, Ministry of Education, School of Chemistry and Chemical Engineering, Henan Normal University, Xinxiang, Henan 453007, P. R. China. E-mail:jwang@htu.cn*

[b]*School of Chemical Engineering and Pharmaceutics, Henan University of Science and Technology, Luoyang, Henan 471003, P. R. China.*

[c]*Bruker China, Beijing Applicat Lab, Beijing 100081, P. R China.*

Table of contents

Experimental Section

Materials

N,N-dimethylethanolamine (99%), 1-methylimidazole (99%), ethanolamine (99.5%), lithium bis(trifluoromethanesulfonyl)imide (99%), 1-ethyl-3-methylimidazolium chloride (99%), 1-chlorodecane (98%), 1-chlorododecane (99%), 1-chlorotetradecane (98%) and 1-chlorohexadecane (97%) were purchased from J&K Chemicals (Beijing, China). Platinum (II) acetylacetonate ($Pt(acac)_2$, 97%) and nitric acid (70 wt% aqueous solution, LC) were acquired from Aladdin (Shanghai, China). All chemicals were used without any further purification.

General procedures for the synthesis and characterization of the ILs

All the ILs used in this work were synthesized according to the procedures described in the literatures. [1] EOAN was synthesized by dropwise addition of nitric acid to equimolar amount of amine at around 0°C under a nitrogen atmosphere. The solution was stirred for 24 hours after addition of the acid. Excess solvent was removed on a rotary evaporator at 50°C in about 3 hours. The final IL was dried several days at reduced pressure in the presence of P_2O_5.

$[C_{10}mim]Cl$ was synthesized by the following procedures. Briefly, 1-chlorodecane was added dropwise into the mixture of 1-methylimidazole and ethyl acetate under stirring, and the mixture was refluxed at 70 ºC. After 48 h, the product was decanted from the hot solution in a separatory funnel and then washed at least 5 times with ethyl acetate. The solvent was evaporated on a rotary evaporator, and the resulting $[C_{10}mim]Cl$ was dried at reduced pressure for at least 72 h. The synthetic procedures of $[C_{12}mim]Cl$, $[C_{14}mim]Cl$, $[C_{16}mim]Cl$, $[C_{12}DMEA]Cl$, $[C_{14}DMEA]Cl$ and $[C_{16}DMEA]Cl$ were the same as that of $[C_{10}mim]Cl$.

$[C_nmim][Tf_2N]$ (n=2, 4, 6, 8, 10) were synthesized by equimolar amount of $[C_nmim]Cl$ and $Li[Tf_2N]$ through metathesis reaction. The crude $[C_nmim][Tf_2N]$ was washed at least 20 times with water until no precipitation was observed with the addition $AgNO_3$. The final $[C_nmim][Tf_2N]$ was dried at reduced pressure for at least 72 h in the presence of P_2O_5.

The above ILs were confirmed by ^{1}H-NMR spectra determined with an AV-400 Bruker spectrometer. Water content in the ILs was less than 0.2% as determined by Karl Fischer titration (Metrohm 851, Switzerland). Melting point (T_m) and thermal decomposition temperature (T_d) of the ILs were measured by means of a differential scanning calorimeter (Netzsch DSC 204F-1, Germany) and a thermogravimetric Analyzer (Netzsch TGA STA449C, Germany), respectively.

Phase diagram measurements

Phase diagrams of the microemulsions were constructed from titration data of the IL surfactants into different concentrations of mixtures of EOAN + $[C_nmim][Tf_2N]$. The IL surfactant was added dropwise by vortexing the mixtures vigorously at 25.0 ± 0.1 °C, and the temperature of the system was controlled with a DC-2006 low temperature thermostat (Hengping Instrument Factory, Shanghai, China). The mass fraction at which turbidity-to-transparency occurred was derived from precise titration data. Based on the critical values obtained at different ratios of EOAN to $[C_nmim][Tf_2N]$, the phase boundary was determined.

DLS measurements

The ILs were first filtered through a 0.22 μm Millopore filter to remove any dust or contaminants. Then, the filtered ILs were used to prepare the samples. After the samples were equilibrated for at least 24h, the size and size distribution of the ILs

mixtures were determined by using a Malvern Zetasizer Nano-90 particle size analyzer (Malvern Instrument Ltd., Worcester, UK) equipped with a solid-state He-Ne (4.0 mW) laser operating at $\lambda = 633$ nm. The scattering angle was set at 90°. Each experiment was carried out in quintuplicate, and the uncertainty in DLS was estimated to be 4%.

Cryo-TEM measurements

The samples were prepared by using a custom-built chamber. After fixation of the TEM grid in the preparation chamber, 5 μL of solution sample was placed on a carbon-coated film supported by a copper grid at room temperature. The grid was quenched rapidly into liquid ethane cooled by liquid nitrogen (-175 °C), and then the sample stored in liquid nitrogen was transferred into a JEOL JEM1400 cryomicroscope. The acceleration voltage was 200 kV, and the working temperature was kept approximately at -175 °C. The images were recorded digitally with a charge-coupled device camera under low-dose conditions.

SAXS measurements

SAXS experiments were performed by using a sealed-tube Cu target (40kV, 40mA) instrument named SAXSess mc^2 (Anton Paar, Austria) which was equipped with a line-collimation Kratky block system and an image plate (IP) detector. Both parts were set in vacuum chamber to avoid air scattering. Viscous liquid sample was loaded into a modified paste cell and heated to high temperature by Anton Paar TCS300 non-ambient stage. Scattering data of sample and background were acquired in a 1h exposure, respectively. Then the background scattering from empty sample holder was subtracted from sample curves after absorption correction. The scattering curves were output as the plot of the scattering intensity (I) vs the scattering vector, $q = (4\pi/\lambda) \sin\theta$ (2θ=scattering angle). The pair-distance distribution function was calculated using the generalized indirect Fourier transform (GIFT) program package.

Stability experiments

The samples were immersed in an oil bath, and the temperature of which was controlled with a SC-15B temperature thermostat (Xinzhi Instrument Factory, Ningbo, China) with an uncertainty of ±0.2ºC. Each sample was kept in the oil bath for at least 1 hour.

Synthesis and characterization of porous Pt

In the preparation of porous Pt, microemulsion of $[C_{12}DMEA]Cl$ + EOAN + $[C_2mim][Tf_2N]$ was used as the high temperature reaction media and template. In a typical synthesis, $Pt(acac)_2$ was dissolved into 3 mL of the IL micromulsion to form $Pt(acac)_2$ solution (2 mM) by maintaining the mixture at 90°C for 1h under stirring. After that, the solution was heated to 180°C and maintained at this temperature for another 8 h without stirring. Then, the obtained porous Pt was washed three times by using an aqueous solution containing 80 wt% of ethanol.

Transmission electron microscopy (TEM) and high resolution transmission electron microscopy (HRTEM) were imaged on a JEOL 2100 transmission electron microscope at an acceleration voltage of 200 kV. TEM measurements were performed by dropping a drop of dilute alcohol solution of the sample on a carbon-coated copper grid and drying at room temperature.

Experimental Results

DSC and TGA results of the ILs

Melting point (T_m) and thermal decomposition temperature (T_d) of the ILs were included in Table S1. As can be seen, all the ILs except for [C_{16}DMEA]Cl had the melting point lower than 100ºC, so that they were belong to the category of ionic liquids. In addition, their thermal decomposition temperature was higher than 226ºC, suggesting that it was possible to prepare high temperature microemulsions by using these ILs.

Table S1. Melting point (T_m) and decomposition temperature (T_d) of the ILs

ILs	T_m (ºC)	T_d (ºC)
EOAN	56	259
[C_2mim][Tf_2N]	-9	440
[C_4mim][Tf_2N]	-4	402
[C_6mim][Tf_2N]	-7	362
[C_8mim][Tf_2N]	-8	345
[C_{10}mim][Tf_2N]	-16	433
[C_{12}mim]Cl	47	272
[C_{14}mim]Cl	68	258
[C_{16}mim]Cl	69	264
[C_{12}DMEA]Cl	92	226
[C_{14}DMEA]Cl	96	230
[C_{16}DMEA]Cl	105	233

Phase behavior of the ternary systems

As shown in Figs. S1 and S2, the immiscible IL mixture [C_{10}mim][Tf_2N] + EOAN was able to compatible by the assistance of IL surfactants ([C_nDMEA]Cl or [$C_n$mim]Cl), and a thermodynamically stable one-phase and two-phase regions were observed in the phase diagram. Comparing the critical lines in the phase diagram, it was clear that the two-phase region slightly expanded when the carbon atomic number in the alkyl chain of ionic liquids surfactants increased from 12 to 14.

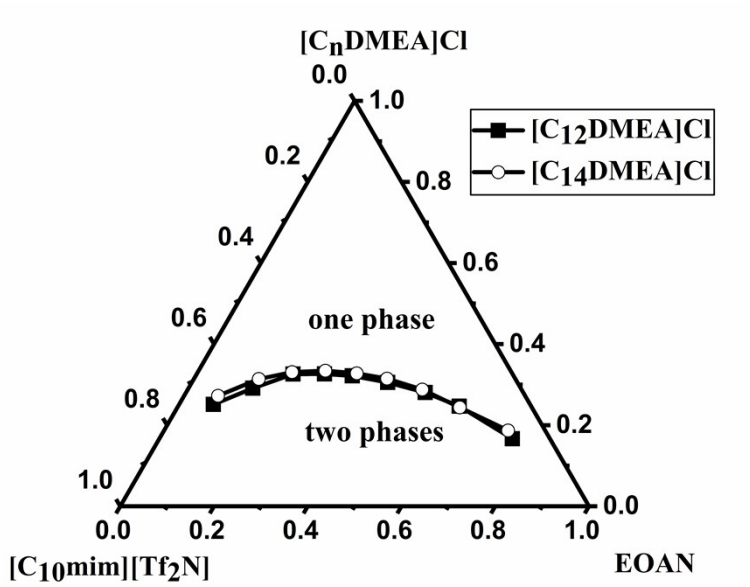

Fig. S1 The ternary phase diagram of EOAN + [C_{10}mim][Tf_2N]+[C_nDMEA]Cl systems at 25ºC.

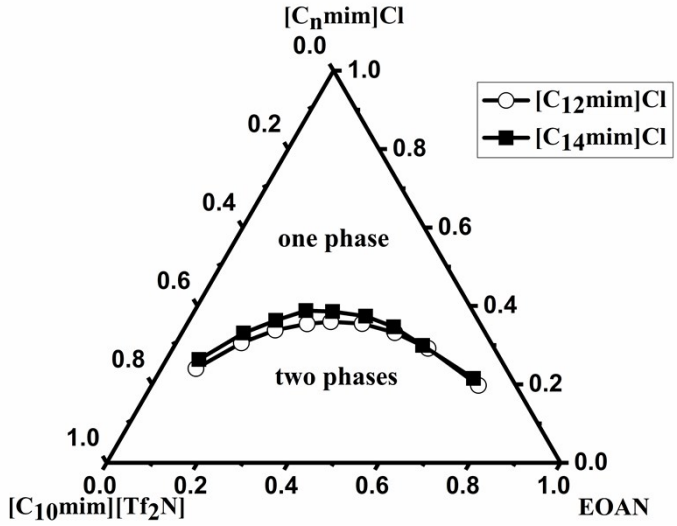

Fig. S2 The ternary phase diagram of EOAN + $[C_{10}mim][Tf_2N]$ + $[C_nmim]Cl$ systems at 25ºC.

Characterization of the microstructures of the ternary systems

In traditional microemulsion studies, DLS have been used to asses if the polar solvent or apolar solvent is encapsulated by surfactants to create micelles or reverse micelles. In this situation, if $[C_nmim][Tf_2N]$ are really encapsulated by the micelles of IL surfactants, size of the droplets must increase with the increase of R value (the molar ratio of $[C_nmim][Tf_2N]$ to the IL surfactant) as well established for traditional microemulsions. On the other hand, if $[C_nmim][Tf_2N]$ are not encapsulated by the IL surfactants, the droplet size will decrease with the increase of R value. The detailed DLS results of microemulsions were shown in Tables S2-S3. It was clear that in these systems, the apparent value in droplets size varied with the R value. For example, two different situations could be observed in EOAN + $[C_{12}mim]Cl$ + $[C_2mim][Tf_2N]$ (S=9.0) system depending on the concentration of $[C_2mim][Tf_2N]$ (or R value). The S here was defined as the mass ratio of EOAN to the IL surfactant. At low $[C_2mim][Tf_2N]$ concentration, the droplet size decreased and then reached the minimum with increasing R value. After that, the droplet size increased with the increase of R value. Therefore, $[C_2mim][Tf_2N]$ could act as a cosurfactant firstly located in the polar-region of interface, leading to a reduction in the droplet size at the lower R value. With the continuous increase of R value, $[C_2mim][Tf_2N]$ was encapsulated into the micelles. The later increase of droplet size indicated swelling behavior of the microemulsion droplets. The same trends were found in other ternary systems as described in Tables S2 and S3.

The DLS results and corresponding cryo-TEM images of the EOAN + $[C_2mim][Tf_2N]$ + $[C_{12}mim]Cl$ systems with different R values were given in Figs. S3 - S5. The results obtained from two different techniques were in good agreement for these microemulsions.

Table S2 The droplet size in EOAN + [$C_n$mim]Cl (n=12,14) + [$C_n$mim][Tf_2N](n=2,10) microemulsions as a function of composition at 25°C

microemulsion	S	R	D(nm)
EOAN+[C_{12}mim]Cl+[C_2mim][Tf_2N]	9.0	0	272
	9.0	0.024	243
	9.0	0.049	231
	9.0	0.066	24
	9.0	0.11	24
	9.0	0.14	21
	9.0	0.15	22
	9.0	0.16	25
	9.0	0.17	44
	19.0	0	437
	19.0	0.050	221
	19.0	0.064	202
	19.0	0.10	103
	19.0	0.11	51
	19.0	0.13	32
	19.0	0.16	38
EOAN+[C_{14}mim]Cl+[C_2mim][Tf_2N]	9.0	0	274
	9.0	0.031	24
	9.0	0.052	20
	9.0	0.086	18
	9.0	0.11	24
	9.0	0.12	37
	19.0	0	221
	19.0	0.054	44
	19.0	0.084	32
	19.0	0.099	41
	19.0	0.11	45
EOAN+[C_{12}mim]Cl+[C_{10}mim][Tf_2N]	9.0	0.051	644
	9.0	0.099	110
	9.0	0.15	23
	9.0	0.20	25
	19.0	0.062	294
	19.0	0.11	191
	19.0	0.13	105
	19.0	0.15	68
	19.0	0.17	29
	19.0	0.18	26
	19.0	0.20	29
	19.0	0.21	32
EOAN+[C_{14}mim]Cl+[C_{10}mim][Tf_2N]	9.0	0	503
	9.0	0.049	338
	9.0	0.099	81
	9.0	0.12	57
	9.0	0.15	25
	9.0	0.16	29
	9.0	0.19	31
	19.0	0.052	560

	19.0	0.087	98
	19.0	0.11	50
	19.0	0.13	36
	19.0	0.15	35
	19.0	0.17	64

Table S3 The droplet size in EOAN + [C_nDMEA]Cl (n=12,14) + [$C_n$mim][Tf_2N] (n=2,10) microemulsions as a function of composition at 25°C

microemulsion	S	R	D(nm)
EOAN+[C_{12}DMEA]Cl+[C_{10}mim][Tf_2N]	9.0	0.050	96
	9.0	0.098	32
	9.0	0.15	26
	9.0	0.17	19
	9.0	0.20	19
	9.0	0.22	21
	9.0	0.25	31
	19.0	0.050	135
	19.0	0.093	33
	19.0	0.12	27
	19.0	0.15	25
	19.0	0.20	23
	19.0	0.22	24
	19.0	0.23	39
	19.0	0.25	75
EOAN+[C_{14}DMEA]Cl+[C_{10}mim][Tf_2N]	9.0	0	41
	9.0	0.048	30
	9.0	0.099	28
	9.0	0.12	26
	9.0	0.17	22
	9.0	0.18	25
	9.0	0.20	35
	9.0	0.21	39
	19.0	0.053	156
	19.0	0.098	100
	19.0	0.12	27
	19.0	0.14	29
	19.0	0.17	42
	19.0	0.20	43

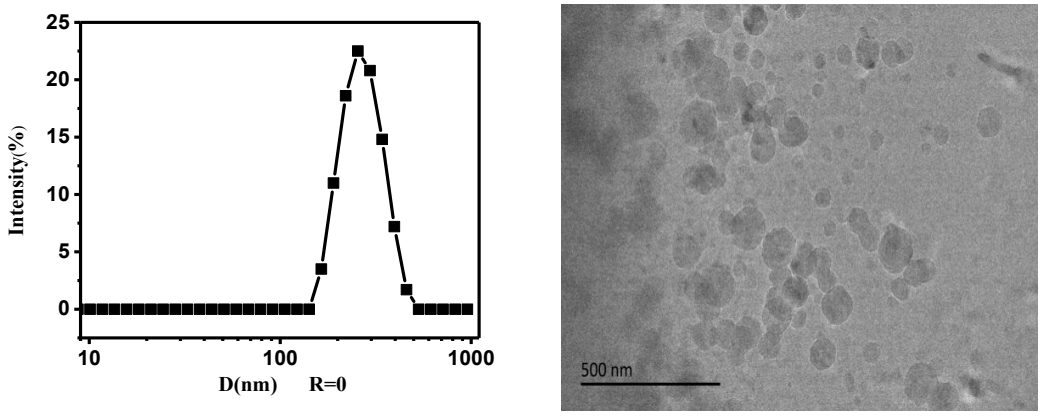

Fig. S3 DLS result and cryo-TEM image of EOAN + $[C_{12}mim]Cl$ (S=9.0, R=0).

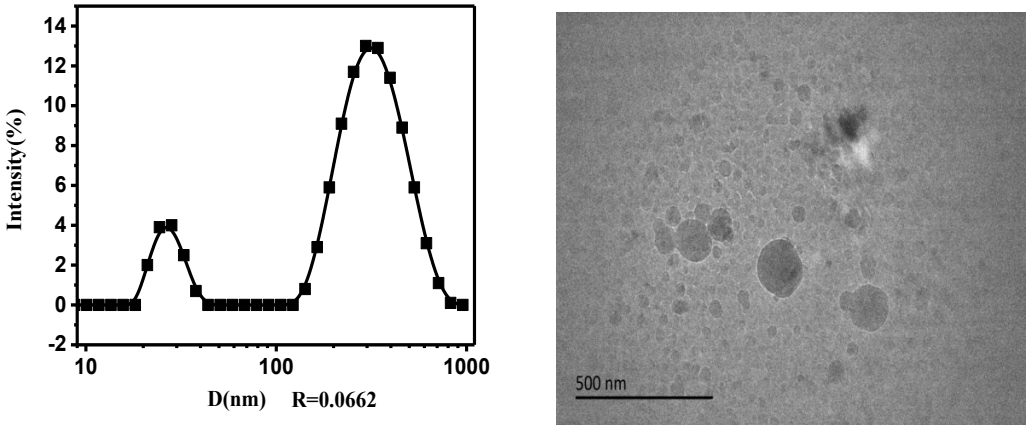

Fig. S4 DLS result and cryo-TEM image of EOAN + $[C_{12}mim]Cl$ + $[C_2mim][Tf_2N]$ system (S=9.0, R=0.066).

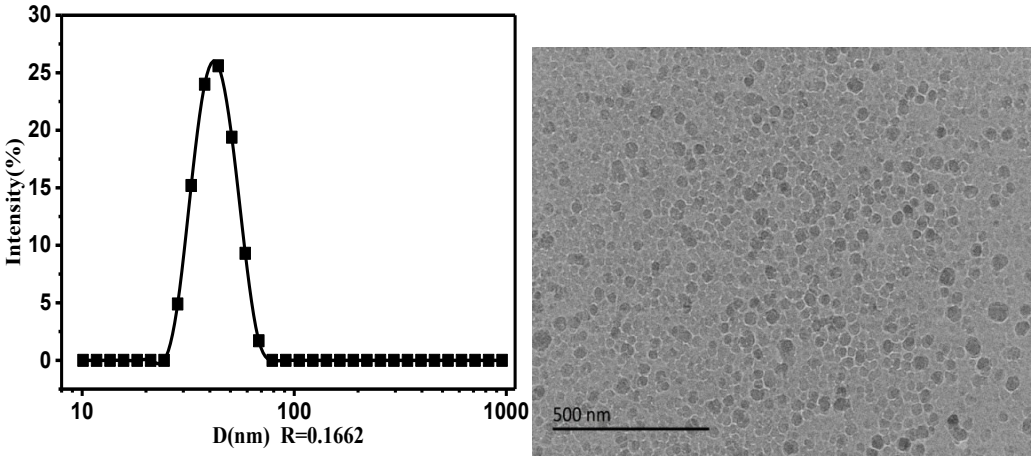

Fig. S5 DLS result and cryo-TEM image of EOAN + $[C_{12}mim]Cl$ + $[C_2mim][Tf_2N]$ system (S=9.0, R=0.17).

High temperature stability

The detailed DLS data of the microemulsions at different temperatures were given in Tables S4 and S5. It was clear that the size of droplets decreased reasonably within a certain range with increasing temperature from 25°C to 92°C at the defined R values. These results suggested that microemulsion droplets were still maintained up to 92°C.

The SAXS results for EOAN + $[C_2mim][Tf_2N]$ + $[C_{12}mim]Cl$ (S=9.0, R=0.17) and EOAN + $[C_2mim][Tf_2N]$ + $[C_{16}mim]Cl$ (S=19.0, R=0.052) systems were given in Figs. S6 and S7. It was found that with increasing temperature from 25°C to 170°C, the p(r) curves in Figs. S6b and Fig. S7b became narrow and the droplet size decreased slightly. This result provided further evidence for the existence of microemulsion droplets at 170°C. Furthermore, it can be seen from Fig.S8 that the microemulsions were still transparent and did not display phase separation even at about 200°C. Therefore, these novel IL-in-IL microemulsions exhibited a wide thermal stability range from room temperature to about 200°C.

Table S4 The size of droplets in EOAN + $[C_nmim]Cl(n=12,14)$ + $[C_2mim][Tf_2N]$ microemulsion at different temperatures

Microemulsion system	S	R	T(ºC)	D(nm)
EOAN+$[C_{12}mim]Cl$+$[C_2mim][Tf_2N]$	9	0.17	25	44
			50	25
			80	24
			92	19
	19	0.10	25	103
			50	15
			80	11
			92	7
	19	0.16	25	38
			50	31
			80	27
			92	23
EOAN+$[C_{14}mim]Cl$+$[C_2mim][Tf_2N]$	9	0.12	25	37
			50	25
			80	22
			92	20
	19	0.11	25	45
			50	39
			80	37
			92	34

Table S5 The size of droplets in EOAN + [C_nDMEA]Cl(n=12,14,16) + [C_2mim][Tf_2N] microemulsion at different temperatures

Microemulsion system	S	R	T(ºC)	D(nm)
EOAN+[C_{12}DMEA]Cl+[C_2mim][Tf_2N]	9	0.11	25	29
			50	15
			80	9
			92	8
	9	0.17	25	19
			50	16
			80	15
			92	12
	19	0.11	50	34
			80	14
			92	10
	19	0.16	25	21
			50	16
			80	13
			92	11
EOAN+[C_{14}DMEA]Cl+[C_2mim][Tf_2N]	9	0.12	25	24
			50	19
			80	15
			92	13
	19	0.11	25	33
			50	31
			80	29
			92	25
EOAN+[C_{16}DMEA]Cl+[C_2mim][Tf_2N]	19	0.063	50	42
			80	39
			92	34

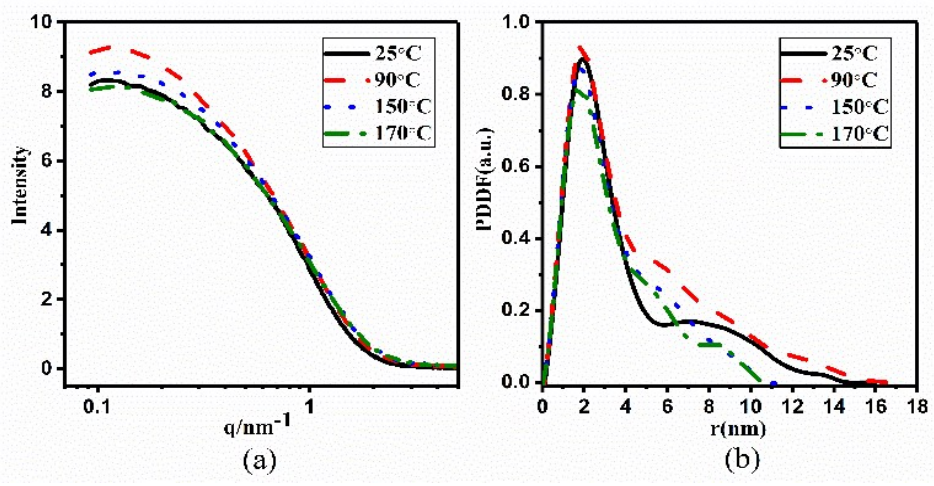

Fig. S6 SAXS (a) and PDDF (b) curves for EOAN + [C_{12}DMEA]Cl + [C_2mim][Tf_2N] microemulsion at different temperatures.

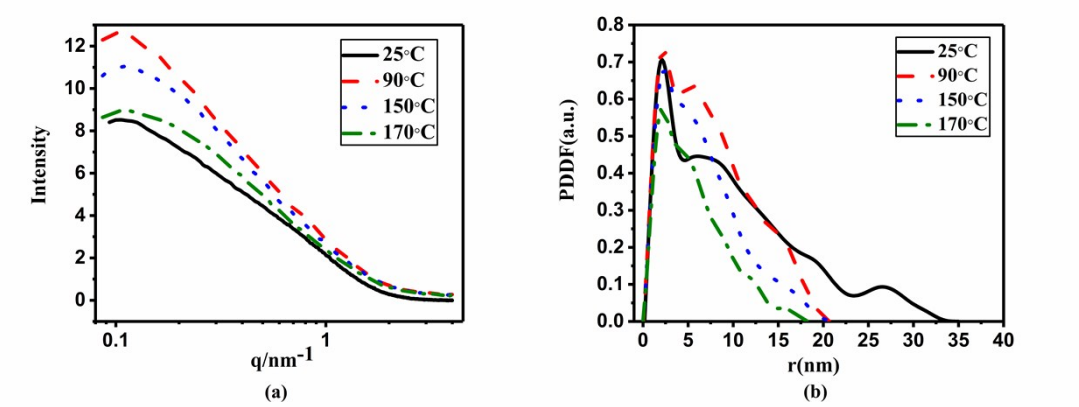

Fig. S7 The SAXS (a) and PDDF (b) curves for EOAN+[C_{12}mim]Cl+[C_2mim][Tf_2N] microemulsion at different temperatures.

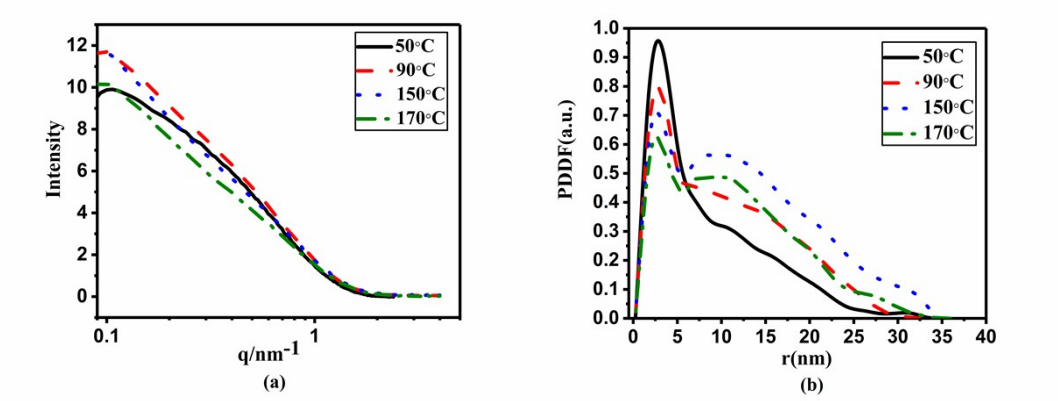

Fig. S8 The SAXS (a) and PDDF (b) curves for EOAN + [C_{16}mim]Cl + [C_2mim][Tf_2N] microemulsion at different temperatures.

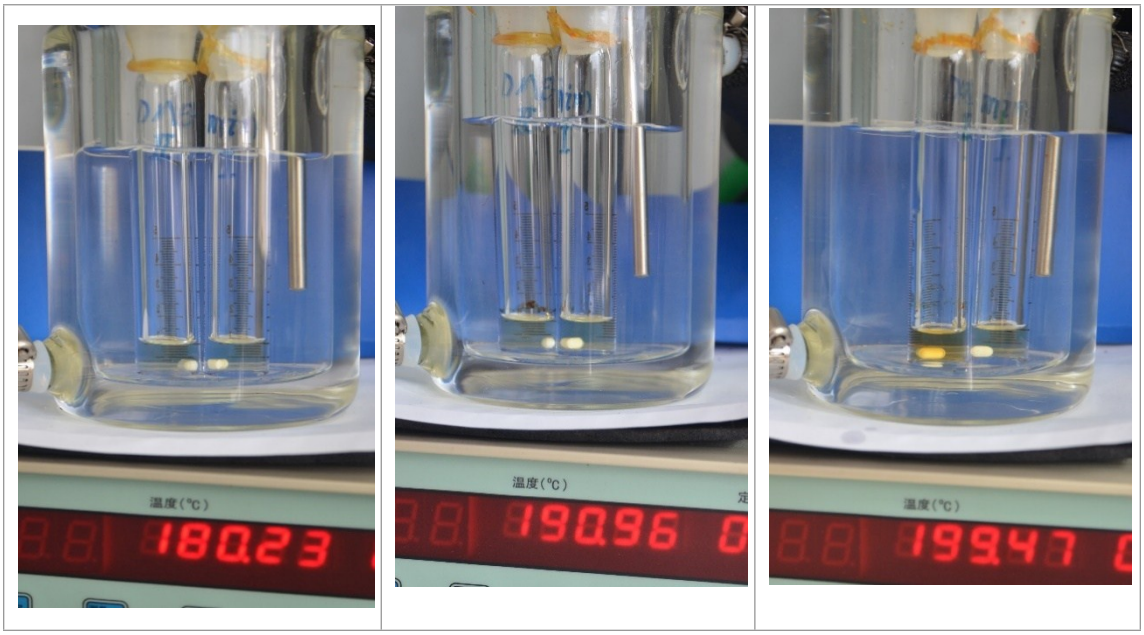

Fig. S9 The pictures of microemulsion systems I and II at different temperatures

References

1. T. L. Greaves, A. Weerawardena, C. Fong, I. Krodkiewska and C. J. Drummond, *J. Phys. Chem., B* 2006, **110,** 22479-22487.